Transactions, SMiRT-23
Manchester, United Kingdom - August 10-14, 2015
Division II, Paper ID 197

TESTS ON SENT SPECIMENS TO STUDY GEOMETRY EFFECTS IN THE BRITTLE TO DUCTILE TRANSITION

Patrick Le Delliou[1], Samuel Géniaut[2]

[1] EDF Research & Development Division, Moret sur Loing, France
[2] EDF, Research & Development Division, Clamart, France

ABSTRACT

The accurate prediction of ductile fracture behaviour plays an important role in structural integrity assessments of critical engineering structures under fully plastic regime, including nuclear reactors and piping systems. Many structural steels and aluminium alloys generally exhibit significant increases in fracture toughness, characterized by the J-integral, over the first few mm of stable crack extension (Δa), often accompanied by large increases in background plastic deformation. Laboratory testing of fracture specimens to measure resistance curves (J–Δa) consistently reveals a marked effect of absolute specimen size, geometry, relative crack size (a/W ratio) and loading mode (tension vs. bending) on R-curves. For the same material, deep-notch bend, SE(B), and CT specimens yield low R-curves while shallow-notch SE(B), single-edge notch tension, SENT, and middle-crack tension, M(T), specimens yield larger toughness values at similar amounts of crack growth.

This paper presents the on-going work to study geometry effects (e.g. triaxiality effects) in the brittle to ductile transition of carbon-manganese steels using SENT specimens, by comparing the results obtained on these specimens with those obtained on CT specimens. A clamped SENT specimen with relative crack depth a/W ≈ 0.5 was chosen for this study. Finite element computations have been made to optimize the specimen shape and to develop the η-factor, the shape factor F (to compute K) and the normalized compliance μ, and preliminary tests have been conducted at room temperature to validate the test procedure.

SENT specimens and CT specimens machined in a 40 mm thick carbon-manganese plate have been tested between -40°C and -100°C. Based on the limited data currently available, no strong geometry effect is evidenced. The Master Curve reference temperature T_0 of the plate in the T-S orientation is close to -70°C. Additional tests will be conducted to adjust the T_0 value and to better appreciate the geometry effect. Finite element analyses of the tests will be conducted with a ductile local approach model coupled with the Beremin model.

INTRODUCTION

The accurate prediction of ductile fracture behaviour plays an important role in structural integrity assessments of critical engineering structures under fully plastic regime, including nuclear reactors and piping systems. Many structural steels and aluminium alloys generally exhibit significant increases in fracture toughness, characterized by the J-integral, over the first few mm of stable crack extension (Δa), often accompanied by large increases in background plastic deformation. Conventional testing programs to measure crack growth resistance (J–Δa) curves employ three-point bend, SEN(B), or compact, CT. However, laboratory testing of fracture specimens to measure resistance curves (J–Δa) consistently reveals a marked effect of absolute specimen size, geometry, relative crack size (a/W ratio) and loading mode (tension versus bending) on R-curves. For the same material, deep-notch bend, SE(B), and CT specimens yield low R-curves while shallow-notch SE(B), single-edge notch tension, SENT, and middle-

crack tension, M(T), specimens yield larger toughness values at similar amounts of crack growth (Figure 1). These effects observed in R-curves have enormous practical implications in defect assessments and repair decisions of in-service structures under low constraint conditions, such as pressurized piping systems with surface flaws (Nyhus, 2003). These crack configurations generally develop low levels of crack-tip stress triaxiality (associated with the predominant tensile loading which develops in pressurized piping systems), thereby contrasting sharply to conditions present in deeply cracked SE(B) and CT specimens.

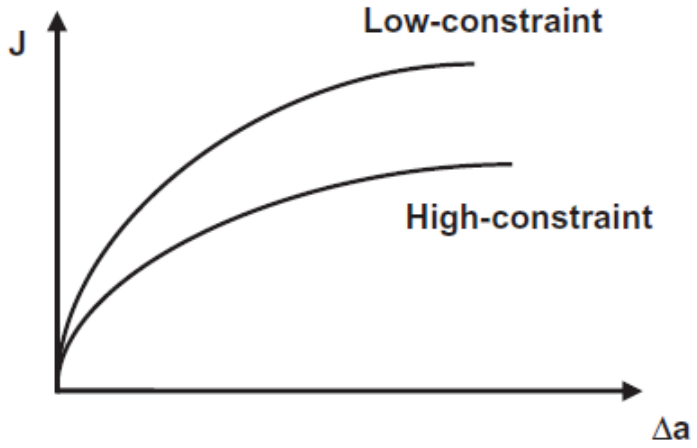

Figure 1. Constraint effect on J-R curves (ductile regime).

This paper presents the on-going work to develop specimens and test procedures to study geometry effects (e.g., triaxiality effects) in the brittle to ductile transition of carbon-manganese steels, the basic idea being to compare the results obtained on these specimens with the results obtained on CT specimens. In a previous work (Le Delliou, 2012), finite element computations were done to optimize the specimen shape and to develop the η-factor, the shape factor F (to compute K) and the normalized compliance μ. Preliminary tests conducted at room temperature with specimens cut in the LS (Long-Short) direction of a carbon-manganese plate, have shown that some adjustments of the test procedure should be made.

New SENT specimens have been machined with shallower notches (a/W = 0.4), to get $a_0/W = 0.5$ after fatigue pre cracking. Fatigue pre cracking was conducted in 4-point bending to avoid damaging the backside of the notch. Moreover, the specimens were cut in the TS (Transverse-Short) direction of the plate to get lower toughness properties, and less plasticity during the tests. Some tests have been conducted at 20°C to check that the procedure is well established in the ductile regime (Le Delliou, 2014).

Finally, tests have been conducted on SENT and CT12.5 specimens in the brittle to ductile region, between -40°C and -100°C. The purpose of the paper is to present the experimental results and to make a comparison of these results.

SPECIMEN DESIGN

The specimen design is fully described in (Le Delliou, 2012) and will not be recalled here. At this design stage, the solutions developed by Cravero (2007) that cover both clamped and pin-loaded specimens were assessed.

Estimation Procedure for the J-integral and Crack Length

The experimental determination of J from the applied load and the crack-opening displacement uses a J estimation scheme, whose main features are recalled herafter.

J is split into an elastic component J_{el} and a plastic component J_{pl}:

$$J = J_{el} + J_{pl} \tag{1}$$

The elastic component J_{el} is computed from the mode I elastic stress intensity factor K_I and the equivalent Young's modulus E':

$$J_{el} = \frac{K_I^2}{E'} \tag{2}$$

where $E' = E/\left(1-\nu^2\right)$ in plane strain and E' = E in plane stress.

The stress intensity factor K_I is defined as follow:

$$K_I = \frac{P}{B\sqrt{W}} F(a/W) \tag{3}$$

where F is a shape factor depending on the relative crack depth a/W.

The plastic component J_{pl} is computed by:

$$J_{pl} = \eta \frac{A_{pl}}{B_N b} \tag{4}$$

where A_{pl} is the plastic area under the load vs. displacement curve, b is the uncracked ligament, B_N is the net thickness. Factor η is a non-dimensional parameter with relates the plastic contribution to the strain energy for the cracked body A_{pl} with J; it is assumed to be a function of the flawed configuration and independent of the loading level.

With the partial unloading method, the computation of J becomes iterative, so for the unloading step k:

$$J_k = J_{el}^k + J_{pl}^k = \frac{K_{I(k)}^2\left(1-\nu^2\right)}{E} + J_{pl}^k \tag{5}$$

$$J_{pl}^k = \left[J_{pl}^{k-1} + \frac{\eta_k}{b_k B_N}\left(A_{pl}^k - A_{pl}^{k-1}\right)\right]\left[1 - \frac{\gamma_k}{b_k}\left(a_k - a_{k-1}\right)\right]$$

where a_k is the crack length at step k, $b_k = W - a_k$ is the uncracked ligament at step k, A_{pl}^k is the plastic area under the load vs. displacement curve at step k.

The γ factor is deduced from the η factor:

$$\gamma_k = \left[-1 + \eta_k - \left(\frac{b_k}{\eta_k} \left.\frac{d\eta}{da}\right|_k \right)\right] \tag{6}$$

During the partial unloading, the compliance C – inverse of the elastic stiffness of the specimen – is computed: $C = \Delta V/\Delta P$, where ΔV is the COD range corresponding to the load range ΔP. The normalized compliance μ is obtained by:

$$\mu = \frac{1}{1+\sqrt{E\, B_{ef}\, C}} \tag{7}$$

where B_{ef} is the effective thickness, equal to B when there are no side grooves. Finally, the relative crack depth is computed from the normalized compliance, thanks to a relation coming from finite element results.

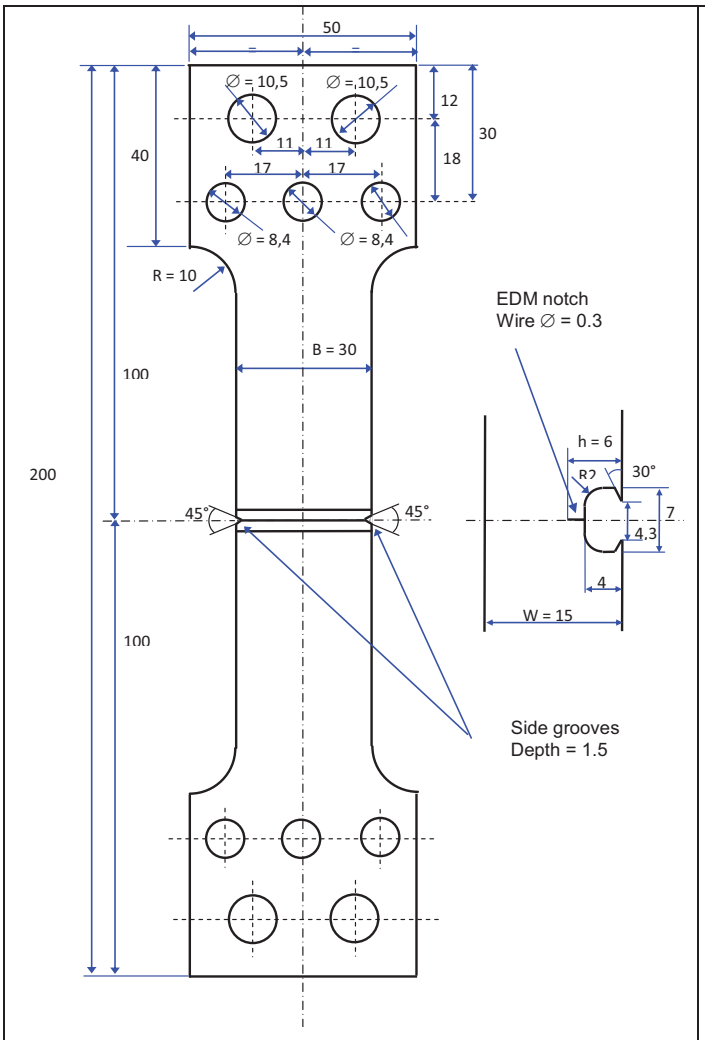

Figure 2. SENT specimen with bolted heads (all dimensions in mm).

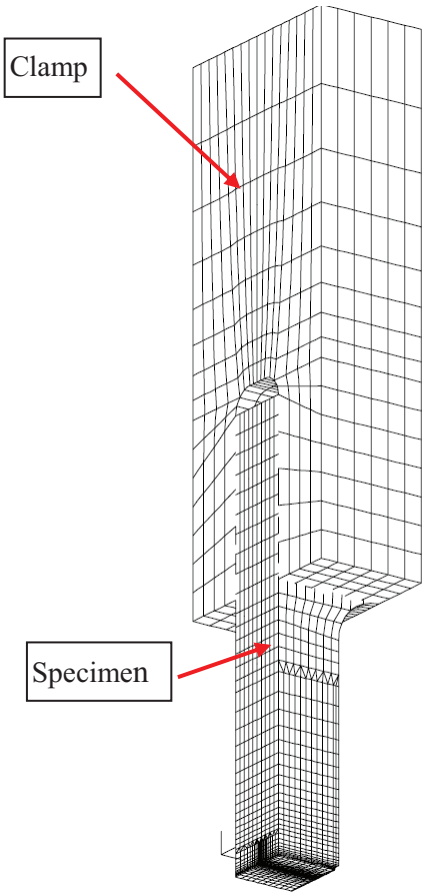

Figure 3. Mesh of the complete specimen with a/W = 0.4.

Specimen Design - Finite Element Models and Computations

In order to be able to machine specimens from schedule 80 16" pipes (outer diameter: 406 mm) whose thickness is around 21 mm, it was decided to fix the thickness W at 15 mm and the width B at 30 mm (over-square shape with B/W = 2). In order to save material, a specimen with heads bolted to clamps was designed (Figure 2), the clamps being themselves gripped into the hydraulic grips of the servo-hydraulic test machine. The H/W ratio of this specimen is around 8 (where H represents the "day-light" between clamps). The specimen is side-grooved at 5 % of B on each side.

A parametric finite element study was conducted to cover a large range of the relative crack depth (a/W ratio). The specimen equipped with its clamps was analyzed, using a tri-dimensional finite element model. Taking into account the symmetries, only one-quarter of the specimen was modeled, with appropriate constraints on the symmetry planes (Figure 3). The bolts are not modeled; instead, they are accounted for thanks to a solid link between elements.

All the calculations were conducted with the FE code Code_Aster (EDF in-house code). Elastic computations were used to develop the relationships between the normalized compliance μ and the

relative crack length a/W, and between the shape factor F and the relative crack length. Nonlinear finite element analyses were conducted with several stress-strain curves to evaluate the factors η and γ needed to compute J. More details about these computations are given in Le Delliou (2012). Only the three formulae needed to analyse the tests are recalled hereafter.

The shape factor is given by the following formula, valid for $0.4 \leq a/W \leq 0.8$:

$$F(a/W) = 0.8895 - 0.7969\,(a/W) + 8.544\,(a/W)^2 \quad (8)$$

The relation between the relative crack length a/W and the normalized compliance μ is given by the following formula, valid for $0.4 \leq a/W \leq 0.8$:

$$a/W = 1.6323 - 7.4965\,\mu + 17.19\,\mu^2 - 17.399\,\mu^3 \quad (9)$$

The η factor can be computed either for the plastic component of the area under the load versus CMOD curve or from the load versus LLD curve, giving respectively η_J^{CMOD} and η_J^{LLD}. Cravero (2007) has shown that for clamped specimens, η_J^{CMOD} decreases steadily and almost linearly between a/W = 0.2 and a/W = 0.6. Accordingly, the linear fit obtained for H/W = 8, valid for $0.4 \leq a/W \leq 0.7$, was retained:

$$\eta_J^{CMOD} = 1.26 - 1.1\,(a/W) \quad (10)$$

EXPERIMENTAL WORK

Specimen preparation

SENT specimens (Figure 4) were machined in a 40-mm thick carbon-manganese plate according to the drawing Figure 2. The specimens were taken in the TS (Transverse-Short) direction of the plate, together with CT12.5 specimens. The EDM notch depth was fixed to 6 mm (a/W = 0.4). The specimens were fatigue pre cracked in 4-point bending (Figure 5), to avoid damaging the backside of the notch. The inner span was reduced to 10 mm, so that the standard 3-point bending formulae can be used (maximum load, elastic compliance and stress intensity factor). The aimed crack depth is 7.5 mm (a_0/W = 0.5).

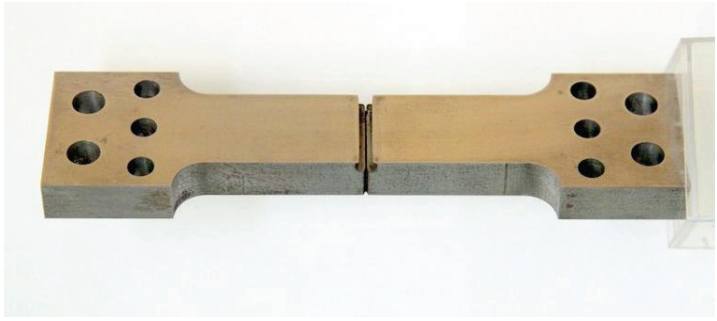

Figure 4. View of the SENT specimen with heads.

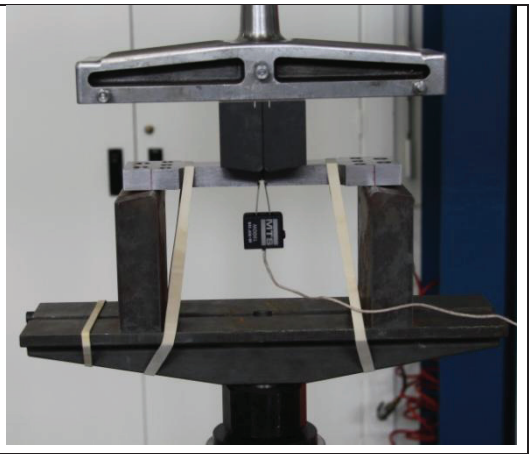

Figure 5. Fatigue precracking in 4-point bending

Room temperature tests

Partial unloading tests were conducted at 20°C on two CT12.5 specimens and on two SENT specimens. CT12.5 test results have shown that the steel has a lower toughness in the TS direction than in the LS

direction, $J_{0.2}$ being close to 150 kJ/m^2 compared to 350 kJ/m^2 in the LS direction. For the SENT, J was computed with the procedure described above. Moreover, for these specimens, following Shen and Tyson (2009), a rotation correction of the compliance was developed by FEA. The details of this development are presented in Le Delliou (2014). The J-R curve of the SENT specimens is slightly above the curve obtained with the CT25.5 specimens, so a moderate "geometry effect" is evidenced.

Low temperature tests

In a first phase, four fracture toughness tests were conducted on CT12.5 specimens, one at -60°C and three at -100°C. At -60°C, the specimen remained ductile so it was decided to test the other specimens at -100°C to obtain a valid K_{IC} value. At -100°C, the K_{IC} value is around 30 $\text{MPa}\sqrt{\text{m}}$ whereas the K_{JC} values range from 51 to 91 $\text{MPa}\sqrt{\text{m}}$. Figure 6 shows the Load-CMOD curves obtained on the four specimens.

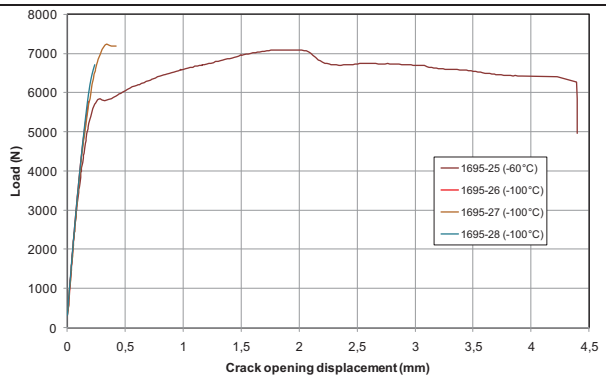

Figure 6. Load versus CMOD curves for the CT12.5 specimens tested at -60°C and -100°C.

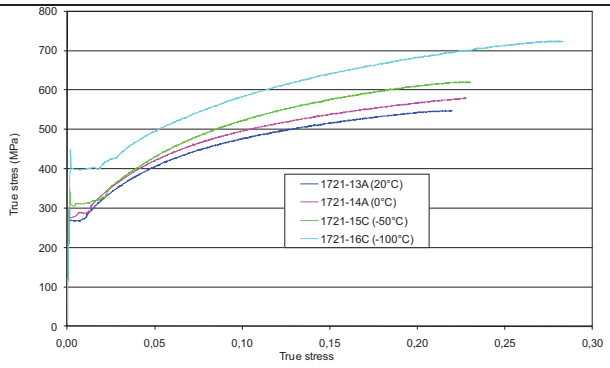

Figure 7. Stress-strain curves of the carbon-manganese steel between 20°C and -100°C.

In order to analyze the tests by FEA, tensile tests were conducted on the carbon-manganese plate at several temperatures between 20°C and -100°C, at a strain rate of 10^{-3}/s. Figure 7 shows the true stress – true strain curves obtained. One can see the strong increase of the tensile properties between -50°C and -100°C. The length of the Lüders plateau seems to increase when the temperature decrease.

Figure 8. View of the SENT specimen in the cold chamber for low temperature tests.

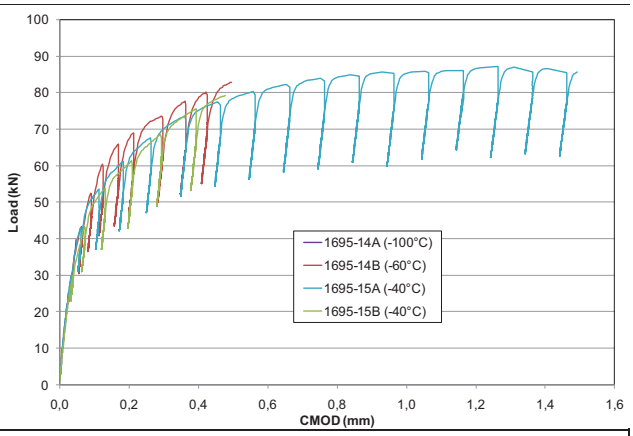

Figure 9. Load versus CMOD curves of the SENT specimens tested at low temperature.

To test the SENT specimens at low temperature, it was necessary to design extra-long clamps, so that these clamps can be tightened into the hydraulic grips outside of the cold chamber (Fig. 8). Four SENT specimens were tested at low temperature (between -100°C and -40°C), using the partial unloading method (Fig. 9). At -100°C, the fracture was brittle. At -60°C and at -40°C, some ductile tearing occurred before brittle fracture. However, even for the specimen 1695-15A showing the largest CMOD at rupture, the ductile extension is moderate (0.96 mm).

In a second phase, to cope with the large scatter observed in the ductile to brittle transition, ten fracture toughness tests were made on CT12.5 specimens, five at -60°C and five at -40°C. Moreover, some tests were conducted according to the single specimen method (partial unloading) and some others according to the multiple specimen method. Fig. 10 and 11 present the load versus CMOD curves obtained at both temperatures. The curve of the specimen 1695-31 is much lower than those of the other specimens, due to an excessive fatigue pre-cracking depth (a_0 = 16.8 mm, for 15 mm nominal). At -40°C, two tests have been interrupted before the occurrence of brittle fracture. The testing procedure (single specimen versus multiple specimen technique) has no significant effect on the results.

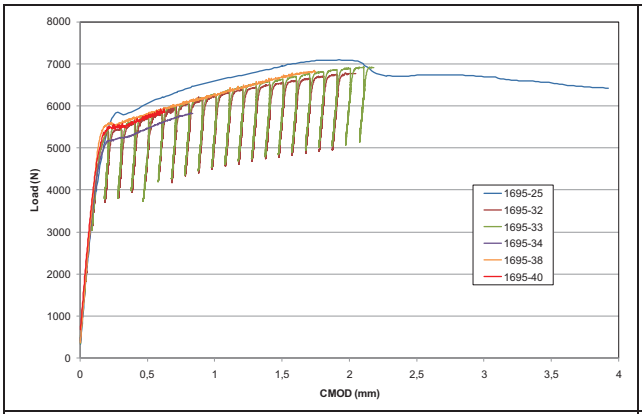

Figure 10. Load versus CMOD curves of the CT12.5 specimens tested at -60°C.

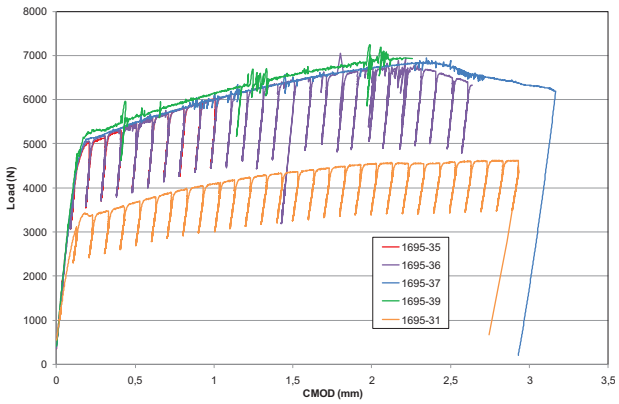

Figure 11. Load versus CMOD curves of the CT12.5 specimens tested at -40°C.

Fig. 12 and 13 show the J-R curves derived from the CT12.5 specimen tests, respectively at -60°C and at -40°C. The tests were analyzed by the multiple-specimen technique, based on the measured final ductile crack extension. At both temperatures, the $J_{0.2}$ value is close to 250 kJ/m^2, the value measured at 20°C being close to 150 kJ/m^2. The decrease of the $J_{0.2}$ value between -60/-40°C and room temperature is likely caused (at least partially) by the decrease of the yield stress with the temperature.

For each specimen, the J-integral value at instability is converted into its equivalent stress intensity factor K_{Jc}. The results of this conversion are shown on Fig. 14. The lowest points are associated with no or very little ductile tearing. The highest points are associated with a significant amount of ductile tearing (from 0.3 mm to 1.55 mm). The points corresponding to the SENT specimens seem to be included in the scatter of the CT12.5 specimen points. Only the point at -100°C is particularly low. However, more SENT specimens must be tested to get a definite conclusion.

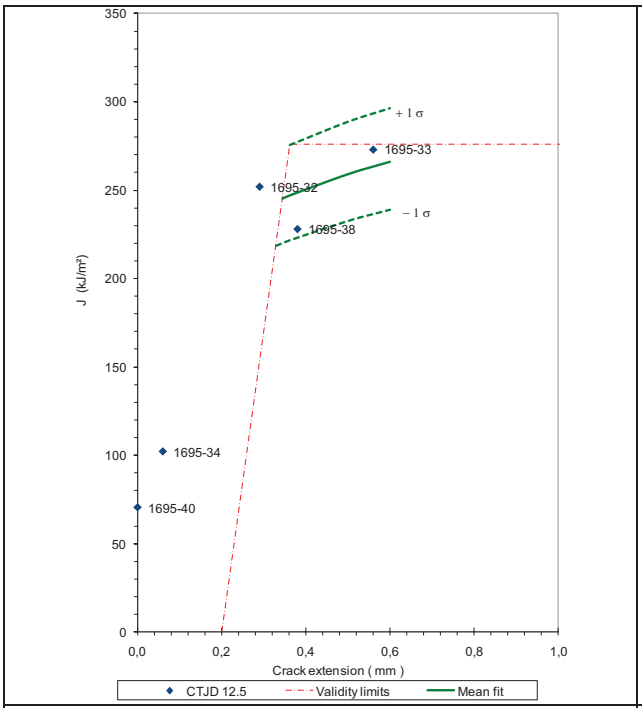

Figure 12. J-R curve fit of the CT12.5 specimens tested at -60°C.

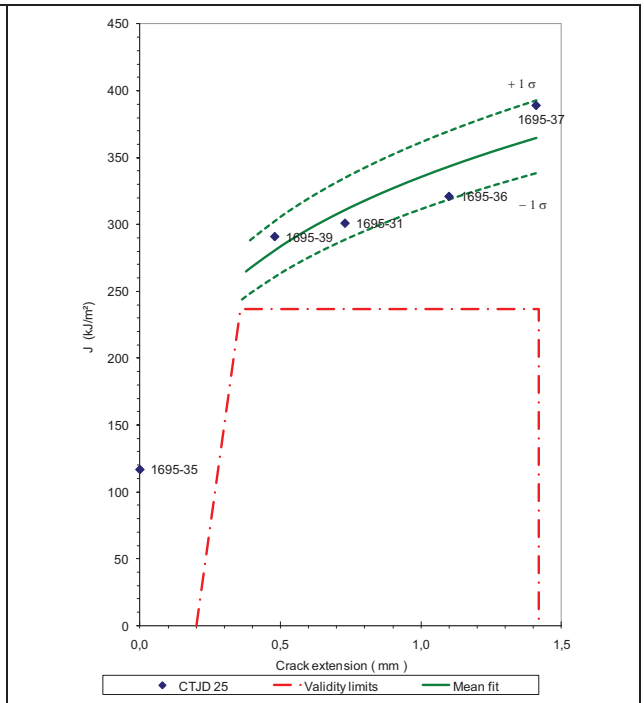

Figure 13. J-R curve fit of the CT12.5 specimens tested at -40°C.

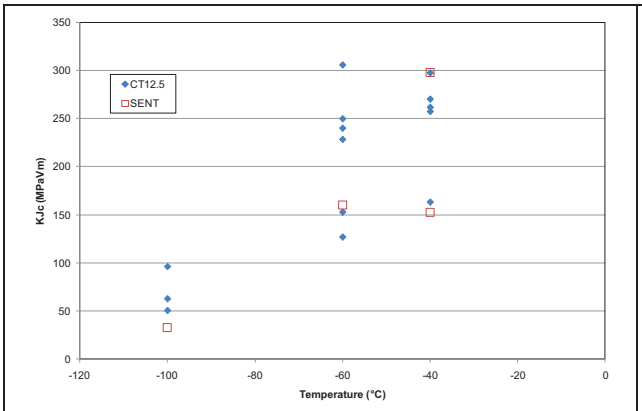

Figure 14. Evolution of the fracture toughness as a function of the test temperature.

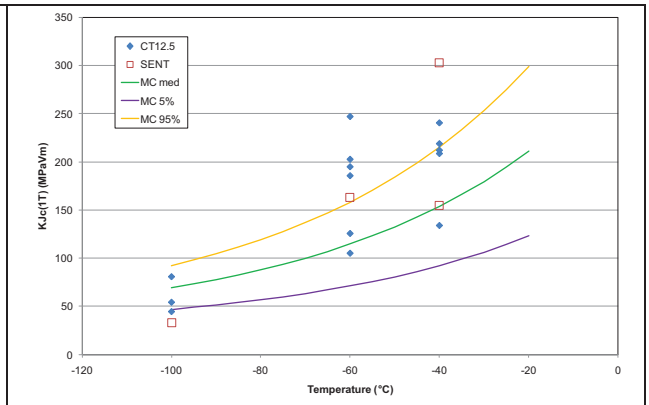

Figure 15. Evolution of the normalised fracture toughness as a function of the test temperature.

ANALYSIS OF THE RESULTS

The experimental results were assessed by the Master Curve approach. The Master Curve gives a universal relationship between the median of the fracture toughness, $K_{Jc(med)}$, and the temperature, T, presented by the following equation:

$$K_{Jc(med)} = 30 + 70\exp\left[0.019\left(T - T_0\right)\right] \qquad (11)$$

where the unit of $K_{Jc(med)}$ is $MPa\sqrt{m}$ and the unit of T and T_0 is °C. T_0 is a reference temperature (such as $K_{Jc(med)} = 100\ MPa\sqrt{m}$ for a 1T CT specimen, i.e. a CT25 specimen) that can be determined by the ASTM E 1921 standard (ASTM, 2008). According to this standard, the raw fracture toughness has to be converted to the "normalised" fracture toughness by the relation:

$$K_{Jc(1T)} = 20 + \left[K_{Jc(x)} - 20\right]\left(\frac{B_x}{B_{1T}}\right)^{0.25} \quad (12)$$

where B_x is the width of the tested specimen and B_{1T} the width of the 1T CT specimen. In our case, the CT12.5 has side grooves, so its net thickness B_N is 10 mm, whereas the net thickness of the SENT specimen is 27 mm. Moreover, the specimen is considered to give a valid K_{Jc} value only if the deformation parameter $M = E\sigma_y b/K_J^2$ is higher than 30, where b is the ligament length and σ_y the yield stress of the steel. In our case, the yield stress is rather low (300 MPa at -50°C) and the ligament is small (10 mm for the CT12.5 specimen and 7.5 mm for the SENT specimen). So this condition is fulfilled only for the specimens showing no ductile tearing. All corresponding data are considered invalid for the determination of the T_0 temperature, but such values can be used in a data censoring analysis, by replacing the measured K_{Jc} by the value obtained by setting M = 30. However, in our case the number of valid specimens is too small to apply the ASTM E 1921 procedure and the T_0 value was set approximately at -70°C, based on the available data (Fig. 15). Additional tests should be conducted at this temperature to adjust T_0. The ASTM standard gives a recommendation relative to the test temperature selection based on the temperature for a Charpy V-notch energy of 28 J, T_{28J}. In our case, T_{28J} was measured in the T-L orientation of the plate at about -10°C. For CT12.5 specimens, the recommended testing temperature is T_{28J} – 28°C, i.e. about -40°C, too high compared with the actual T_0 value.

CONCLUSION

A clamped SENT specimen with heads was designed, and the factors F, μ and η needed to compute J from the experimental load versus CMOD curve were developed, to be used with the unloading compliance technique. The depth of the notch was set at a/W = 0.4, to get a_0/W = 0.5 after fatigue pre cracking. CT12.5 and SENT specimens were cut in the TS (Transverse-Short) direction of a 40 mm thick carbon-manganese steel plate.

Fracture toughness have been conducted on the two types of specimens between -100°C and -40°C in the brittle to ductile region, to put in evidence a possible geometry effect. Based on the limited data currently available, no strong geometry effect is evidenced. The Master Curve reference temperature T_0 of the plate in the T-S orientation is close to -70°C. Additional tests will be conducted to adjust the T_0 value and to better appreciate the geometry effect. Finite element analyses of the tests will be conducted with a ductile local approach model coupled with the Beremin model.

NOMENCLATURE

a	Crack depth
B	Specimen thickness
B_N	Net thickness of a side-grooved specimen
b	Remaining ligament
CT	Compact tension specimen
E	Young's Modulus
H	Net length of a SENT specimen ("Day-light" between grips)
J	J-integral
J_{el}	Elastic component of J-integral
J_{pl}	Plastic component of J-integral
K_J	Elastic-plastic K derived from J
P	Applied load
SENT	Single-edge notch tension specimen
W	Specimen width

Δa Crack extension
γ Non-dimensional factor to account for crack growth effects on J-integral
η Non-dimensional factor, relating the plastic work with the J-integral
μ Non-dimensional compliance
ν Poisson's ratio

REFERENCES

ASTM E 1921-08 (2008). "Standard test method for determination of reference temperature, T_0, for ferritic steels in the transition range", *American Society of Mechanical Engineers*

Cravero, S., and Ruggieri, C. (2007). "Estimation procedure of J-resistance curves for SE(T) fracture specimens using unloading compliance", *Engineering Fracture Mechanics*, 74, pp. 2735-2757

Le Delliou, P., and El-Gharib, J. (2012). "Development of test on SENT specimens to study geometry effects", *Proceedings of ASME 2012 PV&P Conference*, paper PVP#2012-78110

Le Delliou, P., and Géniaut, S. (2014). "Tests on SENT specimens to study geometry effects in the brittle to ductile transition", *Proceedings of ASME 2014 PV&P Conference*, paper PVP#2014-28099

Nyhus, B., Loria Polenco, M., and Ørjasaether, O. (2003). "SENT specimens an alternative to SENB specimens for fracture mechanics testing of pipelines", *Proceedings of OMAE3*, paper OMAE2003-37370

Shen, G., and Tyson, W.R., et al, 2009, "Crack size evaluation using unloading compliance in single-specimen single-edge-notched tension fracture toughness testing", *Journal of Testing and Evaluation*, Vol. 37, No. 4, pp. 347-357

Shen, G., and Tyson, W.R., et al, 2010, "Effect of side grooves on compliance, J-integral and constraint of a clamped SE(T) specimen", *Proceedings of ASME 2010 PV&P Conference*, paper PVP#2010-25164

Xu, J., Zhang, Z.L., Østby, E., Nyhus, B., and Sun, D.B. (2009). "Effects of crack depth and specimen size on ductile crack growth of SENT and SENB specimens for fracture mechanics evaluation of pipeline steels", *International Journal of Pressure Vessels and Piping*, 86, pp. 787-797